Tunable Photonic Radio-Frequency Filter With a Record High Out-of-Band Rejection

Peixuan Li, Xihua Zou, *Member, IEEE*, Wei Pan, Lianshan Yan, *Senior Member, IEEE*, and Shilong Pan, *Senior Member, IEEE*

***Abstract*— As radio-frequency (RF) filtering plays a vital role in electromagnetic devices and systems, recently photonic techniques have intensively been studied to implement RF filters to harness wide frequency coverage, large instantaneous bandwidth, low frequency-dependent loss, flexible tunability, and strong immunity to electromagnetic interference. However, one crucial challenge facing the photonic RF filter (PRF) is the less impressive out-of-band rejection. Here, to the best of our knowledge, we demonstrate a record out-of-band rejection of 80 dB for a tunable PRF with a high processing resolution, by incorporating the highly selective polarization control and the large narrowband amplification enabled by the stimulated Brillouin scattering effect. This record rejection is arduous to be achieved for a narrow passband (e.g., a few megahertz) and a high finesse in a PRF. Moreover, the proposed PRF is an active one capable of providing negligible insertion loss and even signal gain. A tunable central frequency ranging from 2.1 to 6.1 GHz is also demonstrated. The proposed PRF will provide an ultrahigh noise or clutter suppression for harsh electromagnetic scenarios, particularly when room-temperature implementation and remote distribution are needed.**

***Index Terms*— Microwave photonics, out-of-band rejection, photonic radio-frequency filter (PRF), stimulated brillouin scattering (SBS), tunability.**

I. Introduction

HIGH-PERFORMANCE tunable radio-frequency (RF) filters are highly required in electromagnetic devices and systems, such as future 5G wireless communication and beyond, cognitive radio, agile radar, new-generation electronic warfare, and deep-space astronomy [1]–[3]. A large number of architectures and materials have been reported to design and manufacture tunable electronic RF filters [4], [5], to achieve desired specifications for diverse applications and scenarios. In particular, the out-of-band rejection, a key figure of merit of an RF filter, has gained considerable attention for fully suppressing noises, clutters and jamming signals in harsh electromagnetic scenarios. As an example, an out-of-band rejection as high as 80 dB or even 90 dB can be achieved [6]–[11] by using superconductor materials or elements working at an ultralow temperature of 70 K, or dual-mode cavities in the electrical domain. Nevertheless, a wide frequency coverage and a flexible tuning over a large fractional bandwidth are still challenging for these traditional electronic RF filters, due to the limited speed and bandwidth arising from the electronic bottleneck.

Microwave photonics, which combines the RF engineering and optoelectronics [12], [13], takes the intrinsic advantages of photonic technologies to provide basic units or devices [14]–[18] and to enrich or enhance the functions of microwave systems [19]–[35] that are complex or even not directly possible in the electrical domain. Typically, significant functions enabled by microwave photonics include the generation [19]–[21], processing [22]–[24], measurement or detection [25]–[29], and distribution [30]–[37] of microwave signals.

Over the past years, the photonic RF filter (PRF), defined as RF filter assisted by photonics, has shown superior performance in terms of large instantaneous bandwidth, wide frequency coverage, fast frequency tunability, and simple reconfigurability [38]–[56], with respect to the electronic counterparts. However, regarding the out-of-band rejection or signal selectivity that is a key figure of merit for RF filters, the PRFs are generally less competitive for having a value no more than 40 dB in most reports. Here, the out-of-band rejection is defined as the difference between the peak (the maximum) of the noise floor and the transmission peak. There are several exceptional examples with high out-of-band rejection (see more details in Table I). PRFs based on multitap delay line architectures were demonstrated with an out-of-band rejection of ∼70 dB and rapid tunability [38], [39], while providing periodic spectral response. Assisted by cascaded optical resonators, the PRF was able to offer a high out-of-band rejection over 70 dB [42], [43]. By using a Fabry–Perot microresonator, an outstanding rejection of ∼77 dB [43] has been obtained for a much larger passband of 650 MHz. To reduce the passband further to tens or a few megahertz for achieving a high processing resolution or a high finesse, the out-of-band rejection will be degraded by 10 dB or more [43], [45].

In general, however, the maximum out-of-band rejection reported so far for PRFs is still not comparable with the

Manuscript received November 13, 2016; revised February 12, 2017 and March 24, 2017; accepted April 1, 2017. Date of publication May 25, 2017; date of current version November 3, 2017. This work was supported in part by the National "863" Project of China under Grant 2015AA016903 and in part by the National Natural Science Foundation of China under Grant 61378008. The work of X. Zou was supported by a fellowship from the Alexander von Humboldt Foundation, Germany. *(Peixuan Li and Xihua Zou contributed equally to this work.)*

P. Li, X. Zou, W. Pan, and L. Yan are with the Center for Information Photonics and Communications, School of Information Science and Technology, the International Cooperation Research Center of China on Communications & Sensor Networks for Modern Transportation, and also with the National Demonstration Center for Experimental Information Engineering and Technology of Rail Transportation Education, Southwest Jiaotong University, Chengdu 610031, China (e-mail: zouxihua@swjtu.edu.cn; wpan@swjtu.edu.cn).

S. Pan is with the Key Laboratory of Radar Imaging and Microwave Photonics, Ministry of Education, Nanjing University of Aeronautics and Astronautics, Nanjing 210016, China.

Color versions of one or more of the figures in this paper are available online at http://ieeexplore.ieee.org.

Digital Object Identifier 10.1109/TMTT.2017.2693148

TABLE I
SELECTED PRFS WITH REJECTION LARGER THAN 40 dB

PRFs(ref.)	Category	Tunability	Central frequency or frequency coverage (GHz)	3-dB bandwidth (MHz)	Rejection (dB)
47	Notch	Yes	2-20	31	42
41	Notch	Yes	2.5-17.5	6000-9500	~45
55	Notch	Yes	10-40	—	48
46	Notch	Yes	14-20	98	48
54	Notch	Yes	0-50	—	~50
44	Notch	Yes	1-30	33-88	~55
40	Notch	Yes	2-8	247-840	~60
48	Notch	Yes	1-30	10-65	~60
56	Notch	Yes	12.4-30.6	~12500	>60
38	Periodic passbands	—	0.14	~0.44	52/70
39	Periodic passbands	Yes	9.38	170-800	~61/70
49,51	Single passband	Yes	1.6-2.15	250-1000	44/46
52	Single passband	Yes	~8.5	500-3000	45
53	Single passband	Yes	9.68	—	~55
42	Single passband	—	~11.5	650	~70
43	Single-passband	—	—	650	~77
45	Single passband	NO	2.93	3.15	70
This paper	**Single passband**	**Yes**	**2.1-6.1**	**7.7**	**80**

value of state-of-the-art electronic filters based on superconductor materials or elements operating at ultralow temperature (e.g., 70 K in [6]). Therefore, it is extremely challenging to realize PRF with competitively high out-of-band rejection, particularly for the need of fine filtering resolution or high finesse.

Currently, the stimulated Brillouin scattering (SBS) activated in an optical fiber [57] or an on-chip device [58] is used to perform optical and microwave signal processing, such as sensing [59], slow light [60], light storage [61], true time reversal [62], and polarization control [63], with a high resolution due to the ultranarrow bandwidth of the SBS gain or loss. In particular, the SBS can be exploited as a powerful tool to perform RF filtering [44]–[52] with high out-of-band rejection. A notch PRF with an out-of-band rejection higher than 60 dB was achieved based on the SBS in a segment of fiber [48]. By using a Brillouin-active photonic crystal waveguide, an out-of-band rejection of 70 dB was obtained for the PRF with a passband as narrow as 3.15 MHz [45]. However, this filter lacks central frequency tunability, compared with other tunable PRFs with relatively lower rejection [47]. Although these aforementioned SBS-based PRFs are still not competitive with the ultrahigh out-of-band rejection superconducting RF filters, they suggest a great potential to reduce the gap.

Here, we propose a PRF through the combination of the SBS-enabled highly selective polarization control and large narrowband amplification, demonstrating a record high out-of-band rejection up to 80 dB. In the proposed PRF, the incoming RF signal is applied to an electrooptic polarization modulator (PolM) to externally modulate an optical carrier. Under the double-sideband (DSB) modulation, two first-order optical sidebands that are out of phase are generated with the same state of polarization (SOP). But the SOP of the two optical sidebands and that of the optical carrier are orthogonal [64]. Thanks to the unique feature of the polarization modulation by providing orthogonal SOPs between the two sidebands and the optical carrier, the out-of-band noise induced by the phase and amplitude imbalances of two sidebands can be relieved. Furthermore, undesirable signals (e.g., noises or clutters) resulting from the imperfect orthogonality of SOPs, can be canceled as the two optical sidebands are out of phase by 180°. The SBS amplification is used to selectively rotate the SOP of one of the two sidebands and also to boost the amplitude of the same sideband. Therefore, a narrow passband with an ultrahigh out-of-band rejection can be expected. In the experiments, the spectral response of the proposed PRF is measured to achieve a record out-of-band rejection as high as 80 dB. In particular, this record rejection is achieved for a narrow bandwidth of 7.7 MHz and a high finesse of 909, which might be 10 dB or more, higher than that for a passband less than 100 or even 10 MHz [38], [45]. Tunable central frequency is also available for the proposed PRF.

II. PRINCIPLE

The schematic of the proposed PRF is shown in Fig. 1, and the operation principle is presented in Fig. 2. The optical carrier from a laser diode (LD) is split and coupled into two paths. In the lower path, the optical carrier is modulated by the incoming RF signal at the PolM. As illustrated in Fig. 2(a), two first-order optical sidebands that are 180° out of phase are generated with the same SOP which is orthogonal to that of the optical carrier, under the condition of small-signal modulation. In the upper path, the optical carrier is frequency shifted by applying an RF tone with an angular frequency of Ω_p to an intensity modulator (IM) incorporated with an optical bandpass filter (OBPF). The reserved first-order optical sideband is sent to the single-mode fibers (SMFs) at an opposite direction to the polarization-modulated optical signal, to serve as the pump signal. As shown in Fig. 2(b), when the SBS processing is switched OFF, only a direct-current signal

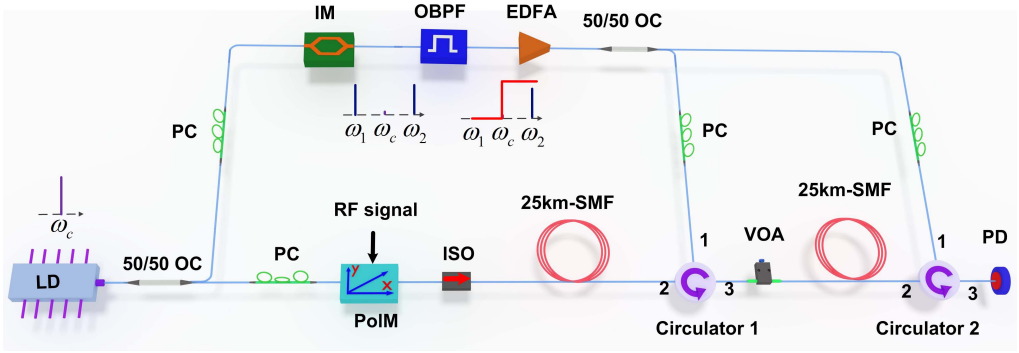

Fig. 1. Schematic of the proposed PRF. (LD: laser diode; OC: optical coupler; PC: polarization controller; MG: microwave signal generator; PolM: polarization modulator; ISO: isolator; SMF: single-mode fiber; IM: Mach–Zehnder intensity modulator; OBPF: optical bandpass filter; EDFA: Erbium-doped fiber amplifier; VOA: variable optical attenuator; PD: photodetector).

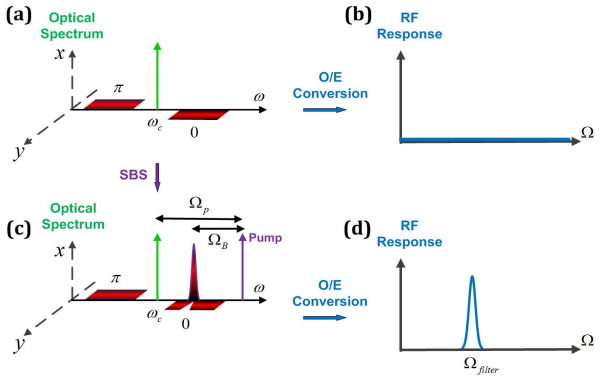

Fig. 2. Illustration of the operation principle of the PRF. Optical spectra of the polarization modulation when switching (a) OFF or (c) ON the SBS processing. RF spectral responses of the PRF when switching (b) OFF or (d) ON the SBS processing. x and y represent two orthogonal polarization axes.

can be detected from the polarization modulation after the optoelectronic conversion, and thus, the spectral response is null in the microwave bands.

Next, the SBS effect is activated to pull the SOP and to boost the amplitude of one of the two optical sidebands generated by applying the incoming RF signal to the PolM. The SOP of the processed optical sideband can be pulled to identically align with that of the optical carrier, as shown in Fig. 2(c). Due to the SBS-induced changes in the SOP and in the amplitude profile of the polarization-modulated optical signal, a conversion from polarization modulation to intensity modulation is realized and consequently the incoming RF signal can be recovered. Furthermore, the SOP control and the amplitude amplification are performed with high selectivity within an ultranarrow-frequency range that is equal to the nature SBS bandwidth. As a result, only the RF signal with one of the corresponding optical sidebands generated by the polarization modulation falling within the SBS bandwidth can be recovered, while other undesired RF components or clutters are removed. Therefore, a single-passband PRF can be realized to achieve an ultrahigh out-of-band rejection. Here, the central frequencies (ω_{gain} and Ω_{filter}) of the SBS gain and the passband of the PRF can be derived as

$$\omega_{\text{gain}} = \omega_c + \Omega_p - \Omega_B \tag{1}$$

$$\Omega_{\text{filter}} = \Omega_p - \Omega_B \tag{2}$$

where ω_c is the angular frequency of the optical carrier, Ω_p is the angular frequency difference between the pump signal and the optical carrier, and Ω_B is the Brillouin frequency shift. From (2), it is clear that the central frequency of the bandpass PRF can be precisely tuned by changing Ω_p.

A. Polarization Modulation

The RF signal here is applied to a commercial AlGaAs/GaAs PolM which is capable of supporting two orthogonal eigen modes. Applying an electrical field to the PolM will induce two equal but out-of-phase changes in the refractive indices along two orthogonal polarization directions of the two eigen modes [65]. When the optical carrier that is linearly polarized at 45° with respect to one principal polarization axis of the PolM is modulated by the incoming RF signal, the electrical field at the output of the PolM can be written as [64]

$$\vec{E}_{\text{PolM}} = \begin{bmatrix} E_x \\ E_y \end{bmatrix} \propto \frac{E_{in}}{\sqrt{2}} \begin{bmatrix} \cos(\omega_c t + \gamma \cos \Omega t) \\ \cos(\omega_c t - \gamma \cos \Omega t) \end{bmatrix} \tag{3}$$

where x and y represent two orthogonal polarization axes which are aligned with the two principal polarization axes of the PolM, E_x and E_y are the decomposed components of the output fields along x and y polarization axes, E_{in} is the amplitude of the optical carrier, and γ is the modulation depth. For simplicity, we assume a sinusoidal RF signal with an angular frequency of Ω. Based on the Jacobi–Anger expansion, (3) can be expressed as

$$\begin{bmatrix} E_x \\ E_y \end{bmatrix} \propto \begin{bmatrix} \cos(\omega_c t)[J_0(\gamma) + 2\sum_{n=1}^{\infty}(-1)^n J_{2n}(\gamma)\cos(2n\Omega t)] \\ -\sin(\omega_c t)\{-2\sum_{n=1}^{\infty}(-1)^n J_{2n-1}(\gamma)\cos[(2n-1)\Omega t]\} \\ \cos(\omega_c t)[J_0(\gamma) + 2\sum_{n=1}^{\infty}(-1)^n J_{2n}(\gamma)\cos(2n\Omega t)] \\ +\sin(\omega_c t)\{-2\sum_{n=1}^{\infty}(-1)^n J_{2n-1}(\gamma)\cos[(2n-1)\Omega t]\} \end{bmatrix} \tag{4}$$

where $J_n(\cdot)$ is the nth-order Bessel function of first kind. For a linear and small-signal modulation, only the

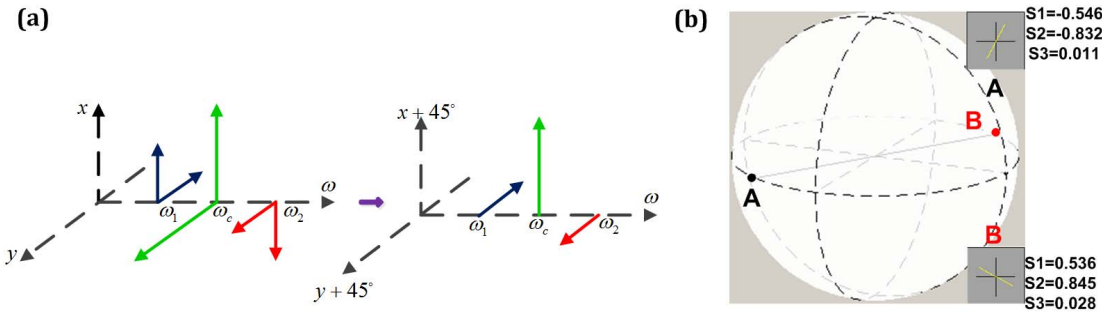

Fig. 3. SOP analysis and measurement for the polarization modulation. (a) Schematic illustration of the phase connection (left) between the two optical sidebands and the optical carrier and the synthesized field vectors (right) for the optical components of the optical carrier and the two optical sidebands along the two orthogonal principal polarization axes of the PolM. (b) Measured SOPs of the optical carrier (marked as A) and the two optical sidebands (marked as B) on the Poincaré sphere. The insets show the measured polarization ellipses and the Stokes vector parameters. Here, x and y represent two orthogonal polarization axes.

first-order sidebands are considered, as schematically illustrated in Fig. 3(a). Thus, (4) can be simplified as (5), shown at the bottom of this page, where m_0 and m_1 denote the amplitudes of the optical carrier and the optical sidebands. Equation (5) demonstrates that the decomposed components for the two optical sidebands at $\omega_1 = \omega_c - \Omega$ and $\omega_2 = \omega_c + \Omega$ along x and y polarization axes are out of phase by 180°, while the decomposed components of the optical carrier along x- and y-axes are in phase. Thus, as shown in Fig. 3(a), the synthesized field vectors for the optical carrier and the two optical sidebands can be derived as

$$\vec{E}_{\text{PolM}} \propto \left\{ \begin{bmatrix} 1 \\ 1 \end{bmatrix} \cos\ (\omega_c t) + \begin{bmatrix} 1 \\ -1 \end{bmatrix} \times \left[\cos\left(\omega_c t + \Omega t + \frac{\pi}{2}\right) - \cos(\omega_c t - \Omega t - \frac{\pi}{2}) \right] \right\}. \tag{6}$$

Note that, the two generated first-order optical sidebands are with the same SOP, but they are out of phase in analog with the feature of a phase modulation (PM) [47]. Moreover, an orthogonal connection is observed between the SOP of the two optical sidebands and that of the optical carrier, as shown in Fig. 3(a). To confirm the connection, the SOPs of the optical sidebands and the optical carrier are measured by a polarization analyzer (PA, Agilent N7788B) and are shown in Fig. 3(b). On the Poincaré sphere, the SOPs of the optical carrier (marked as A) and the two optical sidebands (marked as B) are almost orthogonal, despite a slight deviation due to the limited extinction ratio of the PolM. This slight deviation imposes negligible impact on suppressing undesired RF noises or clutters, due to the nearly orthogonal SOPs between the optical sidebands and the optical carriers. On the other hand, the two out-of-phase optical sidebands can further relieve this unfavorable impact.

B. Polarization Control Using SBS Amplification in Fiber

The SBS amplification in standard, randomly birefringent fibers (typically, standard SMF) is highly polarization-dependent [63], [67] and the corresponding SBS process can be described by the coupled differential equations under the steady state [63]

$$\frac{d\vec{E}_{\text{sig}}^{\text{in}}(z)}{dz} = \left\{ \frac{d\mathbf{R}(z)}{dz}\mathbf{R}^H(z) + \frac{g}{2}\left[\vec{E}_{\text{pump}}(z)\vec{E}_{\text{pump}}^H(z)\right] \right\} \times \vec{E}_{\text{sig}}^{\text{in}}(z) \tag{7}$$

$$\frac{d\vec{E}_{\text{pump}}(z)}{dz} = \left\{ \frac{d[\mathbf{R}^T(z)]^{-1}}{dz}\mathbf{R}^T(z) + \frac{g}{2}\left[\vec{E}_{\text{sig}}^{\text{in}}(z)\vec{E}_{\text{sig}}^{\text{in}H}(z)\right] \right\} \times \vec{E}_{\text{pump}}(z) \tag{8}$$

where $\vec{E}_{\text{sig}}^{\text{in}}(z)$ and $\vec{E}_{\text{pump}}(z)$ are 2×1 matrices denoting the column Jones vectors of the monochromatic SBS probe signal and the pump signal, g is the SBS gain coefficient in unit of $1/(\text{W} \cdot \text{m})$, T and H stand for the transpose operation and the transpose conjugate operation, $\mathbf{R}(z)$ is a Jones matrix describing the fiber birefringence effect, and z is the position along a fiber with a length of L. The probe signal ($\vec{E}_{\text{sig}}^{\text{in}}$) is coupled into the fiber at the position of $z = 0$, while the pump signal ($\vec{E}_{\text{pump}}$) is injected at the position of $z = L$. It is clear that we have two boundary conditions, i.e., $\vec{E}_{\text{sig}}^{\text{in}}(0)$ and $\vec{E}_{\text{pump}}(L)$. To solve the two coupled differential equations, an undepleted pump is assumed such that the power of the probe signal should be small enough to guarantee a negligible impact from the SBS-induced amplification or attenuation to the pump signal. Hence, (8) can be simplified as

$$\frac{d\vec{E}_{\text{pump}}(z)}{dz} = \left\{ \frac{d[\mathbf{R}^T(z)]^{-1}}{dz}\mathbf{R}^T(z) \right\} \vec{E}_{\text{pump}}(z). \tag{9}$$

$$\begin{bmatrix} E_x \\ E_y \end{bmatrix} \propto m_1 \begin{bmatrix} \frac{m_0}{m_1}\cos(\omega_c t) + \cos\left[(\omega_c + \Omega)t + \frac{\pi}{2}\right] - \cos\left[(\omega_c - \Omega)t - \frac{\pi}{2}\right] \\ \frac{m_0}{m_1}\cos(\omega_c t) - \cos\left[(\omega_c + \Omega)t + \frac{\pi}{2}\right] + \cos\left[(\omega_c - \Omega)t - \frac{\pi}{2}\right] \end{bmatrix} \tag{5}$$

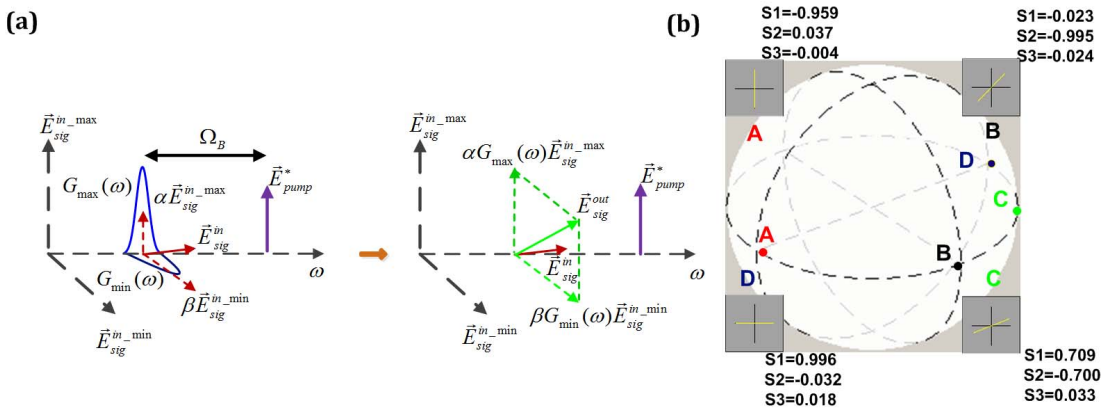

Fig. 4. Polarization control using the SBS. (a) Schematic illustration of the polarization pulling process using the SBS. (b) Measured SOPs of the unprocessed probe signal (marked as A), the polarization-pulled probe signal after the first-stage SBS (marked as B), the pump signal for the first-stage SBS (marked as C), and the polarization-pulled probe signal after the second-stage SBS (marked as D) on the Poincaré sphere. The insets show the measured polarization ellipses and the Stokes vector parameters. The SOP of the probe signal ($\vec{E}_{\rm sig}^{\rm in}$) which falls inside the SBS gain bandwidth is pulled toward that of $\vec{E}_{\rm sig}^{\rm in\_max}$.

With the boundary conditions of $\vec{E}_{\rm pump}(L)$ and $\vec{E}_{\rm sig}^{\rm in}(0)$, $\vec{E}_{\rm sig}^{\rm in}(z)$ can be derived as

$$\vec{E}_{\rm sig}^{\rm in}(z) = \mathbf{A}(z)\vec{E}_{\rm sig}^{\rm in}(0). \tag{10}$$

Subsequently, the probe signal at the end of fiber ($z = L$) can be written as

$$\vec{E}_{\rm sig}^{\rm out} = E_{\rm sig}^{\rm in}(L) = \mathbf{A}(L)\vec{E}_{\rm sig}^{\rm in}(0) \tag{11}$$

where $\mathbf{A}$ is a 2×2 matrix that is determined by the power and the SOP of the pump signal at $z = L$ and by the fiber birefringence. Using the singular value decomposition (SVD) technique, $\mathbf{A}$ can be expressed as

$$\mathbf{A} = \mathbf{U} \cdot \begin{bmatrix} G_1 & 0 \\ 0 & G_2 \end{bmatrix} \cdot \mathbf{V}^H \tag{12}$$

where $\mathbf{U}$ and $\mathbf{V}$ are unitary matrices. According to the theory of the SVD, we generally have $G_1 \geq G_2 \geq 0$. Furthermore, $G_1 > G_2 > 1$ [63] is always satisfied in the case of the SBS amplification. Here, two orthogonal input probe signals are assumed and their Jones vectors are written as

$$\vec{E}_{\rm sig}^{\rm in\_max} = (\mathbf{V}^H)^{-1} \begin{bmatrix} 1 \\ 0 \end{bmatrix} \tag{13}$$

$$\vec{E}_{\rm sig}^{\rm in\_min} = (\mathbf{V}^H)^{-1} \begin{bmatrix} 0 \\ 1 \end{bmatrix}. \tag{14}$$

By substituting (12)–(14) into (11), the output Jones vectors for the two orthogonal input signals can be derived as

$$\vec{E}_{\rm sig}^{\rm out\_max} = \mathbf{U} \cdot \begin{bmatrix} G_1 & 0 \\ 0 & G_2 \end{bmatrix} \cdot \mathbf{V}^H (\mathbf{V}^H)^{-1} \begin{bmatrix} 1 \\ 0 \end{bmatrix} = \mathbf{U} G_1 \begin{bmatrix} 1 \\ 0 \end{bmatrix} \tag{15}$$

$$\vec{E}_{\rm sig}^{\rm out\_min} = \mathbf{U} \cdot \begin{bmatrix} G_1 & 0 \\ 0 & G_2 \end{bmatrix} \cdot \mathbf{V}^H (\mathbf{V}^H)^{-1} \begin{bmatrix} 0 \\ 1 \end{bmatrix} = \mathbf{U} G_2 \begin{bmatrix} 0 \\ 1 \end{bmatrix}. \tag{16}$$

From (15) and (16), it is clear that the two output Jones vectors are orthogonal. In particular, when the condition $G_1 > G_2$ holds, $\vec{E}_{\rm sig}^{\rm in\_max}$ and $\vec{E}_{\rm sig}^{\rm in\_min}$ can provide the maximum and the minimum output power levels for the probe signal, respectively. Then, $\vec{E}_{\rm sig}^{\rm in\_max}$ and $\vec{E}_{\rm sig}^{\rm in\_min}$ can be defined as two orthogonal bases in the vector space. As shown in Fig. 4(a), when the probe signal ($\vec{E}_{\rm sig}^{\rm in}$) and the pump signal are injected into a fiber in opposite directions, an ultranarrow-gain band downshifted by the Brillouin frequency shift Ω_B can be generated in the propagation direction of the probe signal. When the probe signal falls inside the SBS gain bandwidth, this arbitrary polarized probe signal can be decomposed into two components along the two orthogonal bases (i.e., $\vec{E}_{\rm sig}^{\rm in\_max}$ and $\vec{E}_{\rm sig}^{\rm in\_min}$) that denote the maximum and the minimum SBS gains [63]. Then, the optical signal at the output end of the fiber is expressed as

$$\vec{E}_{\rm sig}^{\rm out} = \alpha G_{\rm max}(\omega)\vec{E}_{\rm sig}^{\rm in\_max} + \beta G_{\rm min}(\omega)\vec{E}_{\rm sig}^{\rm in\_min} \tag{17}$$

where α and β are the amplitudes of the two orthogonal components of the input probe signal, $G_{\rm max}(\omega)$ and $G_{\rm min}(\omega)$ denote the maximum and the minimum values of the SBS gain. Generally, for an undepleted pump, we have $G_{\rm max}(\omega) \gg G_{\rm min}(\omega)$ [66] and thus the SOP of the input probe signal can be pulled toward that of $\vec{E}_{\rm sig}^{\rm in\_max}$. Moreover, the SOP of $\vec{E}_{\rm sig}^{\rm in\_max}$ is identical with that of the complex conjugate of the input pump signal [$\vec{E}_{\rm pump}^{*}$ in Fig. 4(a)] [63]. Therefore, the SOP of the probe signal can be controlled in a flexible means by adjusting the SOPs of the pump signal and the SBS gain.

III. Experiments for PRF

The layout and the experimental setup for the proposed PRF are shown in Figs. 1 and 5(a), respectively. A single-wavelength optical carrier with an ultranarrow linewidth (<1 kHz) is generated from a LD (Teraxion PS-TNL) and split into a pump path and a probe path by using a 50:50 optical coupler, one serving as the probe signal and the other as the pump signal. In the pump path, the pump signal is generated by using the carrier-suppressed single-sideband (CS-SSB) modulation. Here, a 40-GHz Mach–Zehnder IM (Sumitomo T.MXH1.5) biased at the minimum transmission point to suppress the optical carrier and an OBPF (Santec OTF-350) with an edge steepness of 75 dB/nm

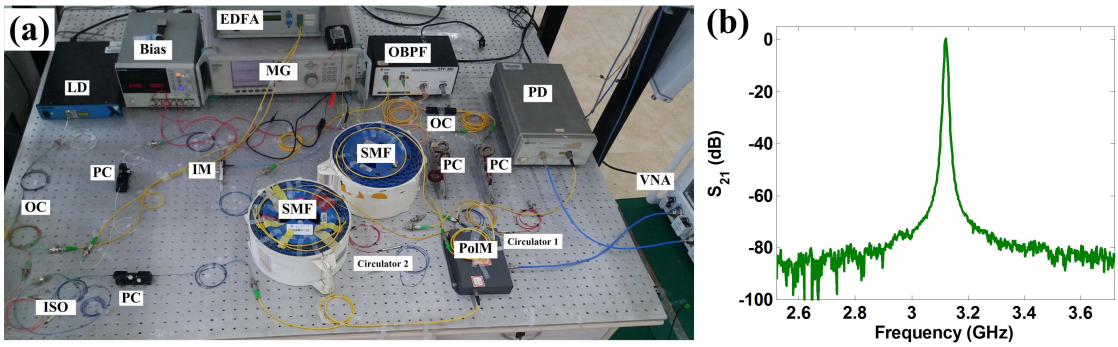

Fig. 5. (a) Photograph of the experimental setup of the proposed PRF. (b) Measured spectral responses (S_{21}) with a signal gain of 0.35 dB. (LD: laser diode; OC: optical coupler; PC: polarization controller; MG: microwave signal generator; PolM, polarization modulator; ISO: isolator; SMF: single-mode fiber; IM: Mach–Zehnder intensity modulator; OBPF: optical bandpass filter; EDFA: Erbium-doped fiber amplifier; VOA: variable optical attenuator; PD: photodetector).

are incorporated to perform the CS-SSB modulation, when a sinusoidal microwave signal at Ω_p is applied. Therefore, the frequency of the pump signal is upshifted by Ω_p. The frequency difference, Ω_p, between the pump signal and the optical carrier in the probe path can be aligned with subhertz precision by controlling a microwave synthesizer. A two-stage SBS architecture is utilized to provide both highly selective polarization control and large amplitude amplification. The pump signal boosted by an Erbium-doped fiber amplifier, is equally split and launched into two 25-km standard SMF spools via optical circulators. Polarization controllers are used to control the SOPs of the pump signals in the two stages to achieve an optimal signal gain. The low-intensity probe signal is coupled into the two fiber spools in an opposite propagation direction with respect to the pump signal for activating the SBS interaction.

The polarization pulling effect of the two-stage SBS in fibers is first verified by analyzing the SOPs, when no RF signal is applied to modulate the optical carrier in the probe path. The pump signal is generated by setting $\Omega_p/2\pi = \Omega_B/2\pi = 10.879$ GHz, which is then amplified to 13 dBm and equally split into the two fiber spools to interact with the probe signal. The SOPs of the pump signal and the probe signal are measured by the PA and are depicted in Fig. 4(b). Without SBS processing on the probe signal, the SOP of the probe signal at port 3 of the first optical circulator (circulator 1) is marked as point A on the Poincaré sphere. Then, the pump signal is switched on to provide the SBS interaction and the SOP of the probe signal after the first-stage SBS is marked as point B. Point C indicates the SOP of the complex conjugate of the pump signal after the first-stage SBS, which was measured at port 3 of circulator 1, when the probe path is switched OFF and only the spontaneous SBS is excited to act as a polarization mirror of the pump signal [66]. Therefore, as shown in Fig. 4(b), the SOP of the probe signal (marked as point A) is pulled toward that of the pump signal (marked as point C). Furthermore, the SOP of the probe signal after the second-stage SBS interaction is measured at port 3 of circulator 2 and marked as point D, showing a detuning of 180° on the Poincaré sphere with respect to its initial SOP (marked as point A).

After the characterization of the SOPs, an incoming RF signal is applied to the PolM (Versawave Technologies) with a bandwidth of 40 GHz and a low half-wave voltage of 3.5 V, to modulate the optical carrier in the probe path for the purpose of filtering demonstration. The pump signal is amplified to have a power level of 13 dBm and equally split into the two fiber spools. The modulated optical signal is then processed by the SBS and sent to a photodetector for optic-electronic conversion. When Ω_p is specified as 14 GHz, a two-port vector network analyzer (Keysight N5232A) is used to measure the spectral response (S_{21}) of the proposed PRF. As shown in Fig. 5(b), a single passband centered at 3.12 GHz is observed, when the pump signal is switched ON. Due to the SBS gain, the proposed PRF is an active one capable of providing signal gain, rather than insertion loss in conventional PRFs. When the power level of the input signal is set as −15 dBm, a signal gain of 0.35 dB is obtained for the passband.

To show more details, the normalized response (dark blue line) is presented in Fig. 6(a). An ultrahigh out-of-band rejection of 80 dB is achieved in a 7-GHz span from 0 to 7 GHz, for the passsband with a 3-dB bandwidth of 7.7 MHz. A zoomed-in view of the passband is also shown in Fig. 6(b). For the purpose of comparison, the spectral response (or the noise floor) is also recorded as the green curve, when the pump signal is switched OFF. Due to the highly selective amplification of the SBS processing, only a slight increase on the noise floor is observed, which is considered as a significant contribution to the achievement of a record out-of-band rejection. To highlight the out-of-band rejection achieved in the proposed PRF, a comprehensive collection on current PRFs with an out-of-band rejection greater than 40 dB is shown in Table I. Here, the achieved 80-dB rejection is one order of magnitude higher than that reported previously [38], [45] for a passband less than 100 MHz or even 10 MHz, enabling an ultrahigh out-of-band rejection under a high processing resolution. Quantitatively, the 80-dB rejection is available for a narrow passband of 7.7 MHz and hence a high finesse of 909.

In general, it is arduous to achieve an ultrahigh rejection for a narrower passband in PRFs, since in the optical domain a high out-of-band rejection is usually accompanied with

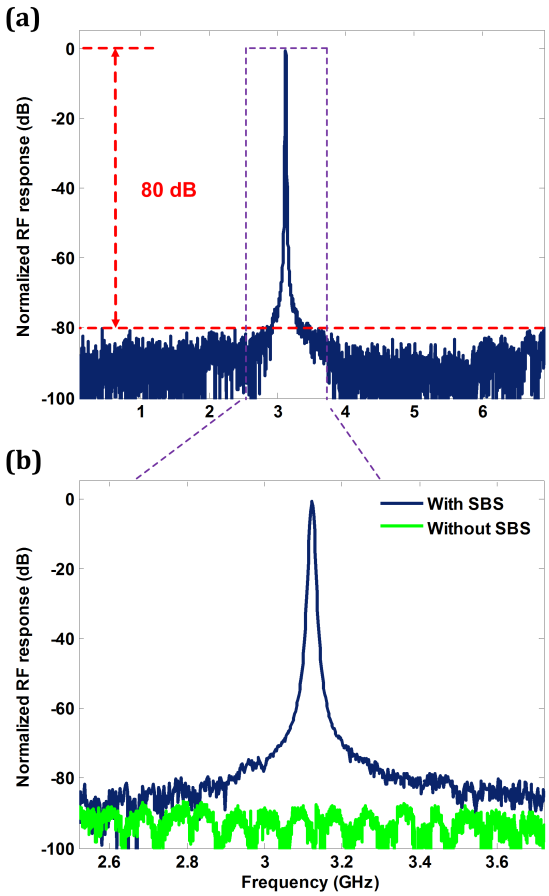

Fig. 6. Measured spectral responses of the proposed PRF. (a) Spectral response centered at 3.1 GHz within a span of 7 GHz, demonstrating an 80-dB rejection. (b) Zoomed-in view of the spectral response within a span of 1.2 GHz by switching ON (dark blue) or OFF (green) the SBS processing.

a wider passband [e.g., dense wavelength division multiplexing devices]. To reduce the passband and to provide a high processing resolution, the out-of-band rejection will be degraded, and vice versa. As an example, when the passband was increased to 650 MHz [43], an optimized value of 77 dB was obtained which can be considered as the maximum out-of-band rejection ever reported for a passband less than 1 GHz. Note that, the maximum value of 77 dB is calculated from the 80-dB rejection stated in [43] by following the definition of the difference between the peak (the maximum) of the noise floor and the transmission peak in this paper. Moreover, the 80-dB out-of-band rejection we achieved is still 3 dB higher than the maximum value of 77 dB ever reported for the PRFs, regardless of the sharp distinction in the passband or the processing resolution. Also, this 80-dB rejection is competitive with the specification of state-of-the-art electronic RF filters operating at stringent ambient temperature (e.g., 70 K for superconducting materials [6]).

It should be mentioned that the architecture of the proposed PRF is close to the classic SBS-based PRF structures [47], [52], but employing a PolM to replace an intensity or phase modulator (PM). However, as aforementioned in the Introduction, it is just the use of a PolM allows us to incorporate the highly selective polarization control and the large narrowband amplification and thus to greatly improve the out-of-band rejection. To clarify this point, advantages and disadvantages about the use of an intensity, phase, or PolM are stated as follows. For the single-sideband/DSB modulation employed in [52], undesired RF components or distortions out of the passband cannot be completely eliminated due to the feature of the intensity modulation, leading to a limited out-of-band rejection. The PM is widely used in the SBS-based PRF for its infinite out-of-band rejection in theory [47]. However, the PM schemes in practice are susceptibly affected by the residual dispersion of the medium (e.g., SMF) and the asymmetric amplitude or/and phase response at the out-of-band frequencies of the photonic devices used. Therefore, the balance between the two first-order sidebands of a PM will be destroyed, resulting in the generation of out-of-band distorts and hence a poor out-of-band rejection. In the proposed PRF, the polarization modulation is used. As the theory description and the experimental results demonstrated in Section II-A, the two first-order sidebands generated are out of phase by 180° , while their SOP are orthogonal with that of the optical carrier. Consequently, we are able to take the advantage of the polarization modulation to achieve a record out-of-band rejection as high as 80 dB.

On the other hand, As predicted in (2), the central frequency of the single passband can be precisely tuned by adjusting Ω_p. Tunable spectral responses centered from 2.1 to 6.1 GHz are obtained with a tuning step of 1 GHz, as shown in Figs. 6 and 7. According to all the measured spectral responses, an ultrahigh out-of-band rejection close to 80 dB can be observed. It should be mentioned that, due to the limited bandwidth with high sensitivity and low noise level of the test instruments, transimpedance amplifier, and optoelectronic devices used in the experiments, the out-of-band rejection will degrade as the central frequency increases. Thus, an ultrahigh rejection is unavailable for high frequencies beyond 10 GHz at this moment. In fact, the frequency coverage will be greatly extended if high-performance test instruments are used.

IV. Discussion

The proposed PRF is demonstrated using discrete optoelectronic devices and fiber spools, which can be considered bulky and of low energy efficiency. But this version of the PRF proposed here can simply be incorporated into existing RF signal processing systems by using commercially available and cost-effective components operating at room temperature, with respect to the ultralow temperature required by the superconductive filters [6]. The use of long fiber link also facilitates remote RF interception in electronic warfare and radar. Furthermore, with the rapid development of the photonic integrated circuit technology [23], [54], it is expected to develop an integrated version of this PRF with a much smaller footprint and a higher power efficiency.

The PRF is also featured by the capability of processing RF or microwave signal with low power level, making it particularly available for applications in cognitive radio, electronic warfare, and deep-space astronomy. There are two reasons

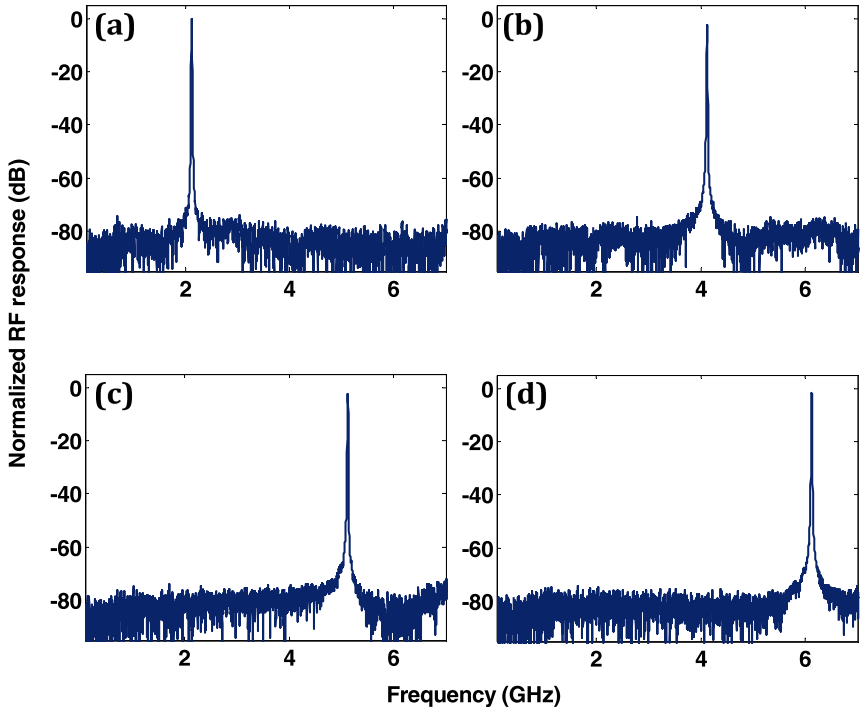

Fig. 7. Demonstration of a tunable central frequency. The spectral responses are measured with a tunable central frequency at (a) 2.1 GHz, (b) 4.1 GHz, (c) 5.1 GHz, and (d) 6.1 GHz. Together with the spectral response centered at 3.1 GHz shown in Fig. 5, a tunable central frequency ranging from 2.1 to 6.1 GHz has been verified experimentally.

behind this capability. First, in order to perform the effective polarization pulling, an undepleted pump regime is generally assumed [49], [63], [66], [68]. Correspondingly, the power level of the probe signal, which is indirectly associated with that of the incoming RF signal, should be sufficiently low. Second, the incoming RF signal with low power level can improve the SBS gain of the proposed PRF, due to the nonlinear behavior of the SBS amplification. Assuming a 10-dBm pump signal, for example, the SBS amplification in a fiber link over 2 km can easily reach the saturated regime by injecting a low-power probe signal less than -40 dBm [70]. In the saturated regime, the output power of the probe signal remains as constant and is insensitive with the power increase of the probe signal. Therefore, in the saturated regime, the relative SBS gain can be improved by decreasing the power level of the probe signal, while keeping a fixed absolute SBS gain. Accordingly, in order to achieve a high SBS gain and hence a high selectivity, a small-signal condition (< -30 dBm) [49], [52], [74] is generally assumed for the operation of the SBS-based PRF. On the other hand, an extremely low power level for the probe signal is unlikely to be applicable, since it will induce strong amplified spontaneous emission (ASE) noise [71], [72].

Another experiment is carried out to further verify the discussions above, according to the theoretical and experimental studies on the linearity of the SBS-based PRFs [69]. When the frequency of the input RF signal is aligned with the central frequency of the proposed PRF, the power of the output RF signal and the signal gain defined as the ratio of the output power to the input power, are measured under different power levels of the input RF signal. As illustrated in Fig. 8(a), the output RF power saturates when the input RF power exceeds -10 dBm, and the signal gain drops rapidly beyond this saturated point. Therefore, an input RF signal with low power level might be considered as an effective method to improve the signal gain and hence the selectivity of the SBS-based PRF. However, a much lower power level might cause other issues, such as the ASE noise contamination to the recovered RF signal [72]. While the power level of the input RF is set as -34 dBm, the recovered RF signal is accompanied by a strong ASE noise which seriously degrades the signal quality and the signal-to-noise ratio (SNR), as shown in Fig. 8(b). In contrast, when the power of the input RF signal is increased to be 4 dBm, the ASE noise is significantly reduced at the cost of the selectivity, as shown in Fig. 8(c). In our PRF system, the power level is set as -15 dBm to relieve the ASE noise while retaining a relatively high signal gain. The measured electrical spectrum of the output RF signal is shown in Fig. 8(d), providing an SNR greater than 30 dB. As a result, a conclusion can be drawn here that a high power level of the input signal can improve the SNR of the recovered RF signal, but might lead to pump depletion and hence a limited signal gain or a limited selectivity, which is identical with that stated in [49]. Therefore, there is a trade-off between the selectivity and the noise contamination, when taking the power of the input RF signal into account.

Besides the ASE noise, the proposed PRF might bring other noises, such as the intensity noise of laser source, the shot and thermal noises of photodetector. Fortunately,

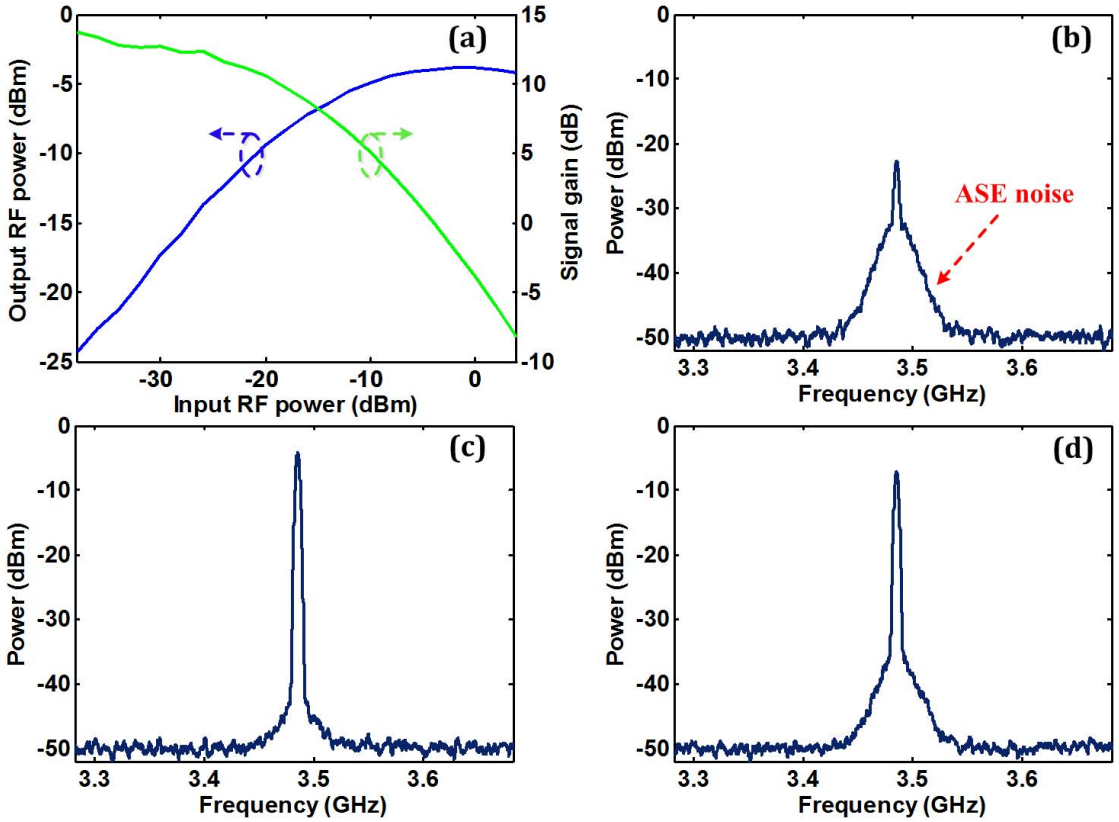

Fig. 8. (a) Measured power of the output RF signal (blue line) and the signal gain (green line) under different power levels of the input RF signal. Measured spectra of the output RF signal when applying an input RF signal of (b) −34 dBm, (c) 4 dBm, and (d) −15 dBm.

for many application scenarios, the noise feature of the proposed SBS-based PRF exerts little negative influence to the system performance. For example, linear-frequency-modulation radar waveforms were successfully processed by the SBS-based PRF to have good integrated sidelobe ratio and peak-sidelobe ratio [73]. In [74], a 2-GHz orthogonal frequency-division multiplexing signal with quadrature-phase shift-keying and 16-quadrature- amplitude-modulation modulations were processed by the SBS-based PRF with negligible error vector magnitude penalty.

V. Conclusion

We have demonstrated a tunable PRF by incorporating the highly selective polarization control and the large narrowband amplification enabled by the SBS effect. The proposed PRF has a record high out-of-band rejection of 80 dB. In particular, the 80-dB rejection is available for a narrow bandwidth of 7.7 MHz, which is one order of magnitude greater than that reported previously for a bandwidth of a few megahertz in PRFs. The proposed PRF is also capable of providing tunable central frequency from 2.1 to 6.1 GHz while remaining at an ultrahigh rejection. Such ultrahigh out-of-band rejection allows the proposed PRF to meet the stringent demands on high selectivity of a target RF signal and on high suppression of noises or clutters in diverse applications such as cognitive radio, electronic warfare, and deep-space astronomy. Furthermore, multiple passbands can be expected by applying a multiple frequency pump [75], to greatly extend the application scope of the proposed PRF.

Appendix

The preprint version of this paper was first posted on the arXiv website [76].

Acknowledgment

The authors would like to thank Prof. J. Yao, Microwave Photonics Research Laboratory, University of Ottawa, Canada, for his comments and suggestions to improve the quality of this paper.

References

[1] R. Levy and S. B. Cohn, "A history of microwave filter research, design, and development," *IEEE Trans. Microw. Theory Techn.*, vol. MTT-32, no. 9, pp. 1055–1067, Sep. 1984.

[2] J. Uher and W. J. R. Hoefer, "Tunable microwave and millimeter-wave band-pass filters," *IEEE Trans. Microw. Theory Techn.*, vol. 39, no. 4, pp. 643–653, Apr. 1991.

[3] R. J. Cameron, R. Mansour, and C. M. Kudsia, *Microwave Filters for Communication Systems: Fundamentals, Design and Applications*. Hoboken, NJ, USA: Wiley, 2007.

[4] A. R. Brown and G. M. Rebeiz, "A varactor-tuned RF filter," *IEEE Trans. Microw. Theory Techn.*, vol. 48, no. 7, pp. 1157–1160, Jul. 2000.

[5] X. Liu, L. P. B. Katehi, W. J. Chappell, and D. Peroulis, "High-Q tunable microwave cavity resonators and filters using SOI-based RF MEMS tuners," *J. Microelectromech. Syst.*, vol. 19, no. 4, pp. 774–784, Aug. 2010.

[6] S. M. I. Tsuzuki, S. Ye, and S. Berkowitz, "Ultra-selective 22-pole 10-transmission zero superconducting bandpass filter surpasses 50-pole Chebyshev filter," *IEEE Trans. Microw. Theory Techn.*, vol. 50, no. 12, pp. 2924–2929, Dec. 2002.

[7] H. Hu and K. L. Wu, "A TM_{11} dual-mode dielectric resonator filter with planar coupling configuration," *IEEE Trans. Microw. Theory Techn.*, vol. 61, no. 1, pp. 131–138, Jan. 2013.

[8] S. Fouladi, F. Huang, D. W. Yan, and R. P. Mansour, "High-Q narrowband tunable combline bandpass filters using MEMS capacitor banks and piezomotors," *IEEE Trans. Microw. Theory Techn.*, vol. 61, no. 1, pp. 393–402, Jan. 2013.

[9] R. H. Olsson, III, J. Nguyen, T. Pluym, and V. M. Hietala, "A method for attenuating the spurious responses of aluminum nitride micromechanical filters," *J. Microelectromech. Syst.*, vol. 23, no. 5, pp. 1198–1207, Oct. 2014.

[10] B. Yassini and M. Yu, "Ka-band dual-mode super Q filters and multiplexers," *IEEE Trans. Microw. Theory Techn.*, vol. 63, no. 10, pp. 3391–3397, Oct. 2015.

[11] *GPS Notch Filter*, accessed on Feb. 12, 2017. [Online]. Available: http://www.reactel.com/pdf/datasheets/6R7-1575-42-X15N11.pdf

[12] A. J. Seeds and K. J. Williams, "Microwave photonics," *J. Lightw. Technol.*, vol. 24, no. 12, pp. 4628–4641, Dec. 2006.

[13] J. Capmany and D. Novak, "Microwave photonics combines two worlds," *Nature Photon.*, vol. 1, no. 6, pp. 319–330, Apr. 2007.

[14] R. C. Hsu, A. Ayazi, B. Houshmand, and B. Jalali, "All-dielectric photonic-assisted radio front-end technology," *Nature Photon.*, vol. 1, pp. 535–538, Aug. 2007.

[15] A. Ramaswamy *et al.*, "Integrated coherent receivers for high-linearity microwave photonic links," *J. Lightw. Technol.*, vol. 24, no. 1, pp. 209–216, Jan. 2008.

[16] A. Stöhr *et al.*, "Millimeter-wave photonic components for broadband wireless systems," *IEEE Trans. Microw. Theory Techn.*, vol. 58, no. 11, pp. 3071–3082, Oct. 2010.

[17] T. R. Clark and R. Waterhouse, "Photonics for RF front ends," *IEEE Microw. Mag.*, vol. 12, no. 3, pp. 87–95, May 2011.

[18] A. Beling, X. Xie, and J. C. Campbell, "High-power, high-linearity photodiodes," *Optica*, vol. 3, no. 3, pp. 328–338, Mar. 2016.

[19] X. S. Yao and L. Maleki, "Optoelectronic oscillator for photonic systems," *IEEE J. Quantum Electron.*, vol. 32, no. 7, pp. 1141–1149, Jul. 1996.

[20] M. H. Khan *et al.*, "Ultrabroad-bandwidth arbitrary radiofrequency waveform generation with a silicon photonic chip-based spectral shaper," *Nature Photon.*, vol. 4, no. 2, pp. 117–122, Feb. 2010.

[21] G. J. Schneider, J. A. Murakowski, C. A. Schuetz, S. Shi, and D. W. Prather, "Radiofrequency signal-generation system with over seven octaves of continuous tuning," *Nature Photon.*, vol. 7, pp. 118–122, Feb. 2013.

[22] S. Tonda-Goldstein, D. Dolfi, A. Monsterleet, S. Formont, J. Chazelas, and J.-P. Huignard, "Optical signal processing in radar systems," *IEEE Trans. Microw. Theory Techn.*, vol. 54, no. 2, pp. 847–853, Feb. 2006.

[23] W. Liu *et al.*, "A fully reconfigurable photonic integrated signal processor," *Nature Photon.*, vol. 10, pp. 190–195, Sep. 2016.

[24] M. Li *et al.*, "Reconfigurable single-shot incoherent optical signal processing system for chirped microwave signal compression," *Sci. Bull.*, vol. 62, no. 4, pp. 242–248, Jan. 2017.

[25] M. Pelusi *et al.*, "Photonic-chip-based radio-frequency spectrum analyser with terahertz bandwidth," *Nature Photon.*, vol. 3, pp. 139–143, Feb. 2009.

[26] T. Bagci *et al.*, "Optical detection of radio waves through a nanomechanical transducer," *Nature*, vol. 507, pp. 81–85, Mar. 2014.

[27] P. Ghelfi *et al.*, "A fully photonics-based coherent radar system," *Nature*, vol. 507, no. 7492, pp. 341–345, Mar. 2014.

[28] M. Burla, X. Wang, M. Li, L. Chrostowski, and J. Azaña, "Wideband dynamic microwave frequency identification system using a low-power ultracompact silicon photonic chip," *Nature Commun.*, vol. 7, Sep. 2016, Art. no. 13004.

[29] X. Zou, B. Lu, W. Pan, L. Yan, A. Stöhr, and J. Yao, "Photonics for microwave measurements," *Laser Photon. Rev.*, vol. 10, no. 5, pp. 711–734, Sep. 2016.

[30] A. S. Daryoush, "Optical synchronization of millimeter-wave oscillators for distributed architecture," *IEEE Trans. Microw. Theory Techn.*, vol. 38, no. 5, pp. 467–476, May 1990.

[31] Y. Li and P. Herczfeld, "Coherent PM optical link employing ACP-PPLL," *J. Lightw. Technol.*, vol. 27, no. 9, pp. 1086–1094, May 1, 2009.

[32] V. J. Urick *et al.*, "Long-haul analog photonics," *J. Lightw. Technol.*, vol. 29, no. 8, pp. 1182–1205, Apr. 2011.

[33] P. J. Matthews, "Analog and digital photonics for future military systems," in *Proc. Opt. Fiber Commun. Conf. (OFC)*, San Francisco, CA, USA, Mar. 2014, Art. no. TH3D-6.

[34] C. Lim, A. Nirmalathas, D. Novak, R. Waterhouse, and G. Yoffe, "Millimeter-wave broad-band fiber-wireless system incorporating baseband data transmission over fiber and remote LO delivery," *J. Lightw. Technol.*, vol. 18, no. 10, pp. 1355–1363, Oct. 2000.

[35] S. Koenig *et al.*, "Wireless sub-THz communication system with high data rate," *Nature Photon.*, vol. 7, no. 12, pp. 977–981, Dec. 2013.

[36] Z. Cao *et al.*, "Advanced integration techniques on broadband millimeter-wave beam steering for 5G wireless networks and beyond," *IEEE J. Quantum Electron.*, vol. 52, no. 1, Jan. 2016, Art. no. 0600620.

[37] T. Nagatsuma, G. Ducournau, and C. C. Renaud, "Advances in terahertz communications accelerated by photonics," *Nature Photon.*, vol. 10, pp. 371–379, May 2016.

[38] E. H. Chan and R. A. Minasian, "Coherence-free high-resolution RF/microwave photonic bandpass filter with high skirt selectivity and high stopband attenuation," *J. Lightw. Technol.*, vol. 28, no. 11, pp. 1646–1651, Jun. 2010.

[39] V. R. Supradeepa *et al.*, "Comb-based radiofrequency photonic filters with rapid tunability and high selectivity," *Nature Photon.*, vol. 6, pp. 186–194, Feb. 2012.

[40] D. Marpaung *et al.*, "Si_3N_4 ring resonator-based microwave photonic notch filter with an ultrahigh peak rejection," *Opt. Exp.*, vol. 21, no. 20, pp. 23286–23294, Oct. 2013.

[41] J. Dong *et al.*, "Compact notch microwave photonic filters using on-chip integrated microring resonators," *IEEE Photon. J.*, vol. 5, no. 2, p. 5500307, Apr. 2013.

[42] A. A. Savchenkov *et al.*, "RF photonic signal processing components: From high order tunable filters to high stability tunable oscillators," in *Proc. IEEE Radar Conf.*, Pasadena, CA, USA, May 2009, pp. 1–6.

[43] A. B. Matsko, W. Liang, A. Savchenkov, V. Ilchenko, D. Seidel, and L. Maleki, "Multi-octave tunable agile RF photonic filters," in *Proc. IEEE Int. Topical Meeting Microw. Photon.*, Noordwijk, The Netherlands, Sep. 2012, pp. 6–9.

[44] D. Marpaung *et al.*, "Low-power, chip-based stimulated Brillouin scattering microwave photonic filter with ultrahigh selectivity," *Optica*, vol. 2, no. 2, pp. 76–83, Feb. 2015.

[45] H. Shin, J. A. Cox, R. Jarecki, A. Starbuck, Z. Wang, and P. T. Rakich, "Control of coherent information via on-chip photonic–phononic emitter–receivers," *Nature Commun.*, vol. 6, Mar. 2015, Art. no. 6427.

[46] A. Casas-Bedoya *et al.*, "Tunable narrowband microwave photonic filter created by stimulated Brillouin scattering from a silicon nanowire," *Opt. Lett.*, vol. 40, no. 17, pp. 4154–4157, 2015.

[47] W. Zhang and R. A. Minasian, "Switchable and tunable microwave photonic Brillouin-based filter," *IEEE Photon. J.*, vol. 4, no. 5, pp. 1443–1455, Oct. 2012.

[48] D. Marpaung, B. Morrison, R. Pant, and B. J. Eggleton, "Frequency agile microwave photonic notch filter with anomalously high stopband rejection," *Opt. Lett.*, vol. 38, no. 21, pp. 4300–4303, Oct. 2013.

[49] Y. Stern *et al.*, "Tunable sharp and highly selective microwave-photonic band-pass filters based on stimulated Brillouin scattering," *Photon. Res.*, vol. 2, no. 4, pp. B18–B25, Aug. 2014.

[50] W. Li, L. X. Wang, and N. H. Zhu, "All-optical microwave photonic single-passband filter based on polarization control through stimulated Brillouin scattering," *IEEE Photon. J.*, vol. 5, no. 4, Aug. 2013, Art. no. 5501411.

[51] S. Preussler, A. Zadok, Y. Stern, and T. Schneider, "Microwave-photonic filters," in *Proc. IEEE German Microw. Conf. (GeMiC)*, Bochum, Germany, Mar. 2016, pp. 61–64.

[52] L. Yi *et al.*, "Polarization-independent rectangular microwave photonic filter based on stimulated Brillouin scattering," *J. Lightw. Technol.*, vol. 34, no. 2, pp. 669–675, Jan. 2016.

[53] J. Liao *et al.*, "A spurious frequencies suppression method for optical frequency comb based microwave photonic filter," *Laser Photon. Rev.*, vol. 7, no. 4, pp. L34–L38, 2013.

[54] J. Sancho *et al.*, "Integrable microwave filter based on a photonic crystal delay line," *Nature Commun.*, vol. 3, Sep. 2012, Art. no. 1075.

[55] Y. Zhang and S. Pan, "Complex coefficient microwave photonic filter using a polarization-modulator-based phase shifter," *IEEE Photon. Technol. Lett.*, vol. 25, no. 2, pp. 187–189, Jan. 2013.

[56] Y. Long and J. Wang, "Ultra-high peak rejection notch microwave photonic filter using a single silicon microring resonator," *Opt. Exp.*, vol. 23, no. 14, pp. 17739–17750, Jun. 2015.

[57] E. P. Ippen and R. H. Stolen, "Stimulated Brillouin scattering in optical fibers," *Appl. Phys. Lett.*, vol. 21, pp. 539–541, Dec. 1972.
[58] H. Shin *et al.*, "Tailorable stimulated Brillouin scattering in nanoscale silicon waveguides," *Nature Commun.*, vol. 4, Jun. 2013, Art. no. 1944.
[59] F. Farahi, C. N. Pannell, and D. A. Jackson, "Potential of stimulated Brillouin scattering as sensing mechanism for distributed temperature sensors," *Electron. Lett.*, vol. 25, no. 14, pp. 913–915, Jul. 1989.
[60] Y. Okawachi *et al.*, "Tunable all-optical delays via Brillouin slow light in an optical fiber," *Phys. Rev. Lett.*, vol. 94, Apr. 2005, Art. no. 153902.
[61] Z. Zhu, D. J. Gauthier, and R. W. Boyd, "Stored light in an optical fiber via stimulated Brillouin scattering," *Science*, vol. 318, pp. 1748–1750, Dec. 2007.
[62] M. Santagiustina, S. Chin, N. Primerov, L. Ursini, and L. Thévenaz, "All-optical signal processing using dynamic Brillouin gratings," *Sci. Rep.*, vol. 3, Apr. 2013, Art. no. 1594.
[63] A. Zadok, E. Zilka, A. Eyal, L. Thévenaz, and M. Tur, "Vector analysis of stimulated Brillouin scattering amplification in standard single-mode fibres," *Opt. Exp.*, vol. 16, no. 26, pp. 21692–21707, Dec. 2008.
[64] A. L. Campillo, "Orthogonally polarized single sideband modulator," *Opt. Lett.*, vol. 32, no. 21, pp. 3152–3154, Nov. 2007.
[65] J. D. Bull, N. A. Jaeger, H. Kato, M. Fairburn, A. Reid, and P. Ghanipour, "40-GHz electro-optic polarization modulator for fiber optic communications systems," *Proc. SPIE*, vol. 5577, pp. 133–143, Dec. 2004.
[66] Z. Shmilovitch *et al.*, "Dual-pump push-pull polarization control using stimulated Brillouin scattering," *Opt. Exp.*, vol. 19, no. 27, pp. 25873–25880, Dec. 2011.
[67] M. O. van Deventer and A. J. Boot, "Polarization properties of stimulated Brillouin scattering in single-mode fibers," *J. Lightw. Technol.*, vol. 12, no. 4, pp. 585–590, Apr. 1994.
[68] A. Wise, M. Tur, and A. Zadok, "Sharp tunable optical filters based on the polarization attributes of stimulated Brillouin scattering," *Opt. Exp.*, vol. 19, no. 22, pp. 21945–21955, Oct. 2011.
[69] M. Pagani, E. H. Chan, and R. A. Minasian, "A study of the linearity performance of a stimulated Brillouin scattering-based microwave photonic bandpass filter," *J. Lightw. Technol.*, vol. 32, no. 5, pp. 999–1005, Mar. 1, 2014.
[70] A. S. Siddiqui and S. Andronikidis, "Transfer characteristics of Brillouin fibre amplifiers for use in self-homodyne coherent optical transmission systems," *Electron. Lett.*, vol. 25, no. 4, pp. 264–266, Feb. 1989.
[71] R. W. Tkach, A. R. Chraplyvy, and R. M. Derosier, "Performance of a WDM network based on stimulated Brillouin scattering," *IEEE Photon. Technol. Lett.*, vol. 1, no. 5, pp. 111–113, May 1989.
[72] M. F. Ferreira, J. F. Rocha, and J. L. Pinto, "Analysis of the gain and noise characteristics of fibre Brillouin amplifiers," *Opt. Quantum Electron.*, vol. 26, no. 1, pp. 35–44, Jan. 1994.
[73] A. Zadok, A. Eyal, and M. Tur, "Gigahertz-wide optically reconfigurable filters using stimulated Brillouin scattering," *J. Lightw. Technol.*, vol. 25, no. 8, pp. 2168–2174, Aug. 2007.
[74] W. Wei, L. Yi, Y. Jaouën, and W. Hu, "Bandwidth-tunable narrowband rectangular optical filter based on stimulated Brillouin scattering in optical fiber," *Opt. Exp.*, vol. 22, no. 19, pp. 23249–23260, Sep. 2014.
[75] E. H. Chan, "Microwave photonic filter with a tunable nonperiodic multiple passband frequency response," *Microw. Opt. Technol. Lett.*, vol. 57, no. 5, pp. 1089–1092, May 2015.
[76] P. Li, X. Zou, W. Pan, L. Yan, and S. Pan. (Nov. 2016). "Tunable photonic radiofrequency filter with an ultra-high out-of-band rejection." [Online]. Available: https://arxiv.org/abs/1611.05553

Peixuan Li received the B.S. degree from Southwest Jiatotong University, Chengdu, China, in 2012, where he is currently pursuing the Ph.D. degree at the School of Information Science and Technology.

His current research interests include photonic microwave signal generation and processing and fiber communication systems.

Xihua Zou (M'10) was a joint training Ph.D. Student with the Microwave Photonics Research Laboratory, University of Ottawa, ON, Canada, from 2007 to 2008, where he was a Visiting Researcher in 2011. In 2012, he joined the Ultrafast Optical Processing Research Group, INRS-EMT, Montreal, QC, Canada, as a Visiting Scholar. Since 2014, he has been a Humboldt Research Fellow with the Institute of Optoelectronics, University of Duisburg-Essen, Germany. He is currently a Full Professor with the Center for Information Photonics and Communications, Southwest Jiaotong University, Chengdu, China. He has authored or co-authored over 80 academic papers in high-impact refereed journals. His current research interests include microwave photonics, radio over fiber, and optical communications.

Dr. Zou was a recipient of the Alexander von Humboldt Research Fellowship, the National Outstanding Expert in Science and Technology of China, the Nomination Award for the National Excellent Doctoral Dissertation of China, the Science and Technology Award for Young Scientist of Sichuan Province, China, and the Outstanding Reviewer of *Optics Communications*. He currently serves as an Associate Editor of the IEEE JOURNAL OF QUANTUM ELECTRONICS, the Guest Editor of the "Special Issue on Microwave Photonics" of the JOURNAL LIGHTWAVE TECHNOLOGY, an Editor and the Coordinator of a "Focus Issue on Microwave Photonics" in the IEEE JOURNAL OF QUANTUM ELECTRONICS, and the leading Guest Editor for a "Special Section on Microwave Photonics" in *Optical Engineering*.

Wei Pan is currently a Full Professor and the Dean of the School of Information Science and Technology, Southwest Jiaotong University, Chengdu, China. He has authored over 200 papers in high-impact refereed journals. His current research interests include semiconductor lasers, nonlinear dynamic systems, and optical communications. He was a Steering and Consultancy Expert of the highest level National Project (973 Project) of China.

Dr. Pan was a recipient of the Academic and Technology Leader of Sichuan Province, China.

Lianshan Yan (S'00–M'04–SM'06) is currently a Full Professor and the Director of the Center for Information Photonics and Communications, Southwest Jiaotong University, Chengdu, China.

Dr. Yan is a Fellow of the Optical Society of America (OSA). He was a recipient of the IEEE Photonics Society Distinguished Lecturer Award during 2011–2013 and the IEEE LEOS Graduate Fellowship in 2002. He served as the Co-Chair or as a TPC member for more than 20 international conferences including the Optical Fiber Communication Conference and Exposition in 2013, the European Conference on Optical Communication in 2013, and the Asia Communications and Photonics Conference during 2010–2012. He currently serves as the Chair of the Fiber Optics Technology Technical Group and the OSA. He was an Associate Editor for the IEEE PHOTONICS JOURNAL.

Shilong Pan (S'05–M'09–SM'13) was a "Vision 2010" Post-Doctoral Research Fellow with the Microwave Photonics Research Laboratory, University of Ottawa, Ottawa, ON, Canada, from 2008 to 2010. He is currently a Full Professor and the Executive Director with the Key Laboratory of Radar Imaging and Microwave Photonics (Ministry of Education), Nanjing University of Aeronautics and Astronautics, Nanjing, China. He has authored or co-authored more than 130 papers in peer-reviewed journals. His current research interests include microwave photonics, which includes optical generation and processing of microwave signals, photonic microwave measurement, and integrated microwave photonics.

Dr. Pan was a recipient of the OSA Outstanding Reviewer Award in 2015. He is currently a Topical Editor of *Chinese Optics Letters*. He was the Chair of numerous international conferences and workshops including as a TPC Chair of the International Conference on Optical Communications and Networks in 2015, a TPC Chair of the High-Speed and Broadband Wireless Technologies Subcommittee of the IEEE Radio Wireless Symposium in 2013, 2014, and 2016, and the Chair of the Microwave Photonics for Broadband Measurement Workshop of the IEEE MTT-S International Microwave Symposium in 2015.